ACS SENSORS

pubs.acs.org/acssensors

Article

Organic Field-Effect Transistor Platform for Label-Free, Single-Molecule Detection of Genomic Biomarkers

Eleonora Macchia, Kyriaki Manoli, Cinzia Di Franco, Rosaria Anna Picca, Ronald Österbacka, Gerardo Palazzo, Fabrizio Torricelli, Gaetano Scamarcio, and Luisa Torsi*

Cite This: *ACS Sens.* 2020, 5, 1822−1830

Read Online

ACCESS | Metrics & More | Article Recommendations

ABSTRACT: The increasing interest in technologies capable of tracking a biomarker down to the physical limit points toward new opportunities in early diagnostics of progressive diseases. Indeed, single-molecule detection technologies are foreseen to enable clinicians to associate the tiniest increase in a biomarker with the progression of a disease, particularly at its early stage. Bioelectronic organic transistors represent an extremely powerful tool to achieve label-free and single-molecule detection of clinically relevant biomarkers. These electronic devices are millimetric in size and in the future could be mass-produced at low cost. The core of the single molecule with a large transistor (SiMoT) platform, based on an electrolyte-gated field-effect transistor, is a gold gate electrode biofunctionalized with a self-assembled monolayer, a densely packed layer of recognition elements. So far, only the SiMoT detection of proteins, using the corresponding antibodies as recognition elements, has been reported. In this study, the SiMoT sensing response toward genomic biomarkers is proposed. Herein, the gate is functionalized with a genomic biomarker for multiple sclerosis (miR-182). This is relevant, not only because a limit of detection of a single molecule is achieved but also because it proves that the SiMoT label-free, single-molecule detection principle is the only one of its kind that can detect, by means of the same platform, both protein and genomic markers.

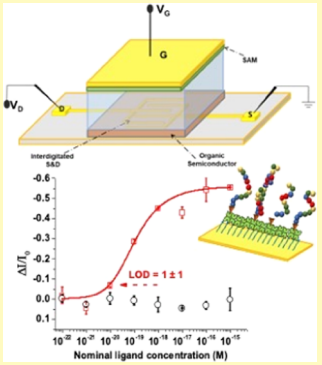

KEYWORDS: *electrolyte-gated organic thin-film transistor, single molecule with a large transistor (SiMoT), genomic markers, biosensors, early diagnosis, DNA detection, miRNAs, multiple sclerosis*

A biomarker is defined as a quantifiable indicator of normal physiological, pathogenic, or pharmacologic responses to a therapeutic intervention.[1] Technologies capable of tracking a biomarker down to the physical limit might open up new opportunities in early diagnostics of progressive diseases. In fact, an assay capable of detecting biomarkers down to the single molecule could quantify the onset of an organism from being "healthy" to being "diseased". Single-molecule biomarker detection would also enable better monitoring of pharmacological therapy as well as the recrudescence of tumors after surgical resection. Moreover, biomarker detection could be carried out noninvasively in peripheral biofluids such as saliva, sweat, tears, and peripheral blood, where biomarkers can be found at much lower concentrations. The development of this approach will pave the way toward ultrasensitive liquid biopsy, instead of the invasive inspection of diseased tissues. From a more fundamental point of view, the sensing of single events faces the ultimate challenge of detecting rare events that would be otherwise lost in the background noise of traditional ensemble measurements.[2−4] The most widespread routine medical testing typically exploits nucleic acids or proteins as clinically relevant biomarkers.[5] In particular, genomic biomarkers, i.e., DNA and RNA, have been extensively used for a range of clinical purposes, such as diagnosis, prognosis, and control over the effect of pharmacological as well as surgical treatments.[6]

The detection of genomic biomarkers has been proposed in 1999,[7] enabling to discriminate between acute myeloid leukemia and acute lymphoblastic leukemia. Since then, a plethora of genomic biomarkers have been proposed to identify alterations to oncogenes that enable early diagnosis of malignant diseases.[8−10] Among the plethora of genomic biomarkers, microRNAs (miRNAs) are defined as noncoding RNA molecules that play a number of crucial roles in cellular and developmental processes by regulating gene expression at the post-transcriptional level. In particular, miRNAs are endogenous single-stranded RNAs, holding a length of approximately 22 nucleotides and regulating up to one-third of all human protein-coding genes.[11] In fact, miRNAs are involved in pivotal processes such as cell proliferation and differentiation, apoptosis, oncogenesis, metabolism, and

Received: April 5, 2020
Accepted: June 4, 2020
Published: June 4, 2020

https://dx.doi.org/10.1021/acssensors.0c00694
ACS Sens. 2020, 5, 1822−1830

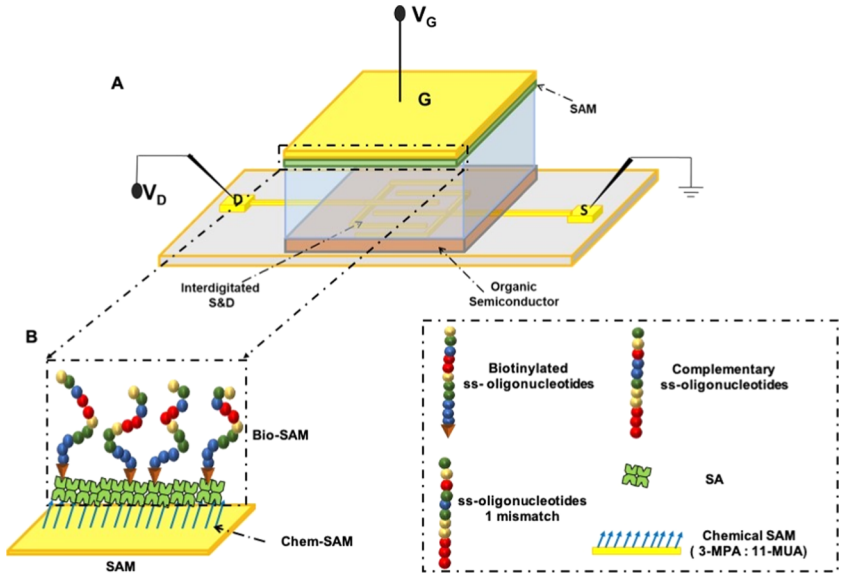

Figure 1. (A) Three-dimensional schematic representation of the SiMoT device. (B) Schematic representation of the gate surface biofunctionalized with a biotinylated single-strand oligonucleotide. Chem-SAM is depicted by blue arrows, and the structures of bio-SAM and target oligonucleotides (miR-182-5p) are sketched in the right panel.

inflammations.[12] Dysregulation of miRNA expression and function leads to a plethora of human diseases such as cancer, neurodegeneration, and autoimmunity.[13,14] Recently, an aberrant miRNA expression profiling has been demonstrated in multiple sclerosis (MS) patients with respect to healthy controls.[15] MS is one of the most common neurological disorders in young adults characterized by dysregulated immune mechanisms. The disease manifests as acute focal inflammatory demyelination with incomplete remyelination and axonal loss, which gradually provokes multifocal sclerotic plaques in the white matter of the central nervous system.[16] These plaques give rise to various cognitive and functional impairments. The identification of biomarkers in body fluids of patients with MS is nowadays driving intensive efforts to elucidate the underlying disease mechanisms, disease progression, and therapeutic response. As miRNAs are present in stable forms in peripheral body fluids, such as human blood and plasma, and their expression profile can be investigated, all of these make them ideal MS biomarker candidates.[17] Indeed, peripheral blood constituents of MS patients have been compared to those of healthy controls in recent miRNA expression profiles studies, demonstrating a large number of differentially expressed miRNAs. Such an analysis has been performed for the first time by Siegel et al., revealing significant involvement of miRNAs in MS and suggesting that miRNAs may serve as potential prognostic and diagnostic biomarkers for MS.[18] This study was able to classify six plasma miRNAs, which were significantly upregulated, and one that was significantly downregulated in MS patients. Later on, Keller et al. found that 16 miRNAs were downregulated and 22 miRNAs were upregulated, by means of next-generation sequencing (NGS) and microarray analysis to test the whole blood from MS patients.[19] Among the differentially expressed miRNAs in MS patients, several studies indicate a critical contribution of miR-182 to the regulation of helper T cell population expansion.[20,21] However, the main effort is still required to master technological aspects of miRNA detection, aiming at high throughput, sensitivity, and accurate analysis. In fact, the level of miRNAs in real biofluids is very low and thus an efficient and reproducible detection of miRNA can be a challenging task to achieve.[9] In fact, given the short length and high sequence similarity of different miRNAs' families, reliable and sensitive detection has not been achieved so far.

The polymerase chain reaction (PCR) represents the workhorse for nucleic acid detection.[22,23] PCR assays can be performed directly on genomic DNA samples with a sensitivity of just a few copies of a nucleic acid sequence. However, PCR needs multiple steps to be completed and this is acknowledged as a limitation to its applicability outside a clinical laboratory environment. Besides, large amplification of contaminants is also an issue. PCR has recently developed into Ion Torrent next-generation sequencing (NGS) technology to overcome some drawbacks of conventional PCR.[24] Ion Torrent registers a pH change, by means of an ion-selective metal−oxide−semiconductor field-effect transistor (MOSFET), when a nitrogenous base of a given DNA fragment is "recognized" by means of the polymerase enzyme. Ion Torrent is capable of detecting 15 molecules. However, Ion Torrent is always accompanied by the need for multiple steps and hence an increase in the assay time. Indeed, 3−5 h or even a few working days are necessary to complete the assay.[25]

Recently, single-molecule, label-free detection has been accomplished by means of a millimeter-wide bioelectronic electrolyte-gated transistor, addressed as a single molecule with a large transistor (SiMoT).[26−29] The SiMoT platform has been proven to perform label-free selective detection at the physical limit in real biofluids of protein biomarkers, such as human Immunoglobulin G[26,30] and Immunoglobulin M,[27] C-reactive protein,[28] and HIV1 p24 antigen.[31,32] The general approach engaged in the biofunctionalization procedure to attach the recognition elements to the transducing electrode makes the SiMoT platform suitable for the detection of different classes of markers. Herein, the SiMoT principle is proposed to detect genomic biomarkers at the physical limit using a strand comprising a sequence of nucleotides complementary to those of the biomarker as the probe recognition element. In particular, a proof of principle for the detection of a single copy of a strand of a nucleotide sequence complementary to

https://dx.doi.org/10.1021/acssensors.0c00694
ACS Sens. 2020, 5, 1822−1830

miR-182-5p is successfully achieved with the SiMoT platform. Moreover, the high selectivity of the SiMoT platform has been proven by performing a negative control experiment when a probe with a single mismatch is used. This is a first successful proof of principle of label-free, cost-effective, fast, and highly selective detection of genomic biomarkers down to the physical limit. Due to the highest specificity toward both genomic and protein markers along with a detection limit of one single molecule, the SiMoT platform paves the way for point-of-care early diagnostic of numerous solid malignancies, such as multiple sclerosis and lung, colon, and breast cancer, among others. Moreover, the present study proves that the SiMoT detection principle is the only one that can be used to detect, with the same single-molecule platform, both protein and genomic markers.

EXPERIMENTAL SECTION

Materials. Poly(3-hexylthiophene-2,5-diyl) (P3HT) organic semiconductor (OSC) with regioregularity >99%, molecular weight 17.5 kDa (g mol^{-1}), is purchased from Sigma-Aldrich. The organic semiconductor was used with no further purification. 3-Mercaptopropionic acid (3-MPA), 11-mercaptoundecanoic acid (11-MUA), 1-ethyl-3-(3-dimethylaminopropyl)-carbodiimide (EDC), and *N*-hydroxysulfosuccinimide sodium salt (sulfo-NHS) were purchased from Sigma-Aldrich and used with no further purification. Streptavidin (SAV) from *Streptomyces avidinii* lyophilized from 10 mM potassium phosphate was purchased from Sigma-Aldrich and used with no further purification. Oligonucleotides were purchased from Eurofins Genomics and readily used. Biotinylated oligonucleotides (sequence 5′-AGTGTGAGTTCTACCATTGCCAAA) were used as biorecognition elements, while the following sequence TTTGGCAATGGTAGAACTCACACT was used as the target oligonucleotides. Water (high-performance liquid chromatography (HPLC) grade, Sigma-Aldrich) and ethanol-grade puriss. p.a. assay, ≥99.8%, were used with no further purification. The phosphate-buffered saline (PBS, Sigma-Aldrich) solution presents osmolality and ion concentrations matching those of the human body (isotonic). One tablet of PBS is dissolved in 200 mL of water (HPLC grade), resulting in 0.01 M phosphate buffer, 0.0027 M potassium chloride, and 0.137 M sodium chloride, pH 7.4, at 25 °C.

Electrolyte-Gated Organic Thin-Film Transistor Fabrication. The electrolyte-gated organic thin-film transistor (EG-OTFT), shown in Figure 1A, was fabricated starting from a silicon substrate (n-doped) with thermally grown SiO_2 (300 nm thick) on top. The SiO_2 surface was cleaned using an ultrasonic bath in acetone and 2-propanol for 10 min. Source (S) and drain (D) interdigitated electrodes were then photo-lithographically defined on the Si/SiO_2 substrate. Afterward, an adhesion layer of titanium (thickness 5 nm) and then a gold layer (thickness 50 nm) were deposited by means of electron beam evaporation. The distance between two fingers is addressed as the channel length (L = 5 μm), and the perimeter of each set of equipotential fingers is defined as the channel width (W = 7650 μm). The substrate with the interdigitated electrodes was cleaned through a procedure involving sonication in 2-propanol, and then, the deposition of the organic semiconductor was performed. A P3HT solution (2.6 mg mL^{-1} in chlorobenzene) filtered with a 0.2 μm filter was spin-coated at a speed of 2 × 10^3 rpm for 20 s and annealed at 90 °C for 15 min. A polydimethylsiloxane well was attached across the electrode channel area, and then, 300 μL of water (HPLC grade), serving as the electrolyte solution, was poured into the well. A Kapton foil, having an area of ∼0.6 cm^2, with e-beam-evaporated gold (50 nm) on titanium (5 nm) on top of it was used as the gate (G) electrode. The gate was stably positioned on water on top of the well in correspondence to the electrode interdigitated area. We note that P3HT can be deposited by means of low-cost printing techniques, for example, ink-jet, aerojet, and electrohydrodynamic jet,[33−35] thus enabling the fabrication of printed EG-OTFTs on large-area and flexible substrates.

Gate Biofunctionalization Protocol. The gate electrodes were cleaned by means of sonication in 2-propanol for 10 min, subsequently rinsed with HPLC-grade water, dried with N_2, and then treated for 10 min in an ozone cleaner. The gate biofunctionalization protocol, described elsewhere in detail[36] and schematically represented in Figure 1B, involves as the first step the immobilization of a chemical SAM (chem-SAM) on the gold surface comprising 10 mM solution of 3-MPA and 11-MUA (10:1 molar ratio) in ethanol. The cleaned gold surface was dipped inside the 3-MPA and 11-MUA solution and kept in the dark under constant N_2 flux for 18 h at 22 °C. The resulting monolayer will be addressed in the following as chemical SAM (chem-SAM). The strong gold−sulfur interaction results in the exposure of carboxylic groups, activated subsequently by reacting the gate electrode in an aqueous solution of 200 mM 1-ethyl-3-(3-dimethylaminopropyl) carbodiimide (EDC) and 50 mM sulfo-*N*-hydroxysuccinimide (sulfo-NHS) for 2 h at 25 °C. The gate surface with activated carboxylic groups was immersed in an SAV phosphate-buffered saline (PBS) solution for 2 h at 25 °C. The solution comprises 1.5 μM (0.1 mg mL^{-1}) SAV in PBS at pH 7.4. Afterward, to saturate the unreacted sulpho-NHS groups, the SAV SAM was further treated with 1 M ethanolamine in 10 mM PBS for 1 h at 25 °C. Finally, the gate was then immersed in a biotinylated single-strand oligonucleotide sequence solution for 2 h at 25 °C. The solution was composed of 0.5 μM biotinylated single-strand oligonucleotide sequence (5′-AGTGTGAGTTCTACCATTGCCAAA), complementary to miR-182-5p, in the PBS solution at pH 7.4. Eventually, after each step of the biofunctionalization, the gate was washed with the corresponding solvent to remove the possible unbounded residues. In the text, we will adopt the following notation: SAM is relevant to the layer comprising both chem-SAM and bio-SAM. Taking into account the gate electrode area and the molecular weight of a single-stranded oligonucleotide, a number of ∼10^{12} capturing receptor particles are assumed to be immobilized on the gate surface.

Sensing Measurements. Sensing measurements have been performed following the experimental protocol described in a previous article.[26] The transistor transfer curves have been recorded with a semiconductor parameter analyzer in air and at room temperature (20−22 °C). Before measuring the sensing signal source−drain current (I_D), this is stabilized by measuring the subsequent transfer curves (I_D vs the gate bias V_G at a fixed source−drain bias V_D) of the electrolyte-gated organic TFT with a gold gate until three transfer curves perfectly overlap. The bare gold gate is here addressed as the "reference" gate, but it is not an electrochemical reference electrode. A functionalized gate has been then measured, instead of the bare gold gate used for the stabilization, and incubated (at RT and in the dark) for 10 min in 100 μL of PBS. After removing the gate from the PBS solution, it was washed thoroughly with HPLC-grade water, and the source−drain current, addressed as the baseline (I_0), was recorded. The same gate was subsequently incubated for 10 min in 100 μL of PBS standard solutions of the analyte sequence of the oligonucleotides with nominal concentrations ranging from 1 × 10^{-2} zM (10^{-21} M) to 10 × 10^8 zM. The PBS solution mimics the environment of blood serum, having a pH of 7.4 and an ionic strength of 162 mM. The target single-strand oligonucleotide (miR-182-5p) is complementary to the probe attached to the gate, thus presenting the following sequence: TTTGGCAATGGTAGAACTCACACT. After each incubation in the PBS standard solutions of miR-182-5p starting from the more diluted one, the gate was rinsed with PBS and water (HPLC grade) to remove unbound molecules, and the relevant I−V transfer curves were registered. The stable currents measured after incubation in the assayed standard solutions are addressed as the signal "I" at a certain concentration. $\Delta I/I_0 = [(I - I_0)/I_0]$ is the normalized response at a given concentration, and the relevant dose−response or calibration curve is obtained by plotting these data at the V_G value that maximizes the transconductance $\delta I_D/\delta V_G$ (being estimated in the −0.3 to −0.4 V range), for all of the inspected concentrations. As a negative control, dose−response curves involving the detection of an analyte, which is the target strand with one single mismatch (TTTGGCAATGGTA-

https://dx.doi.org/10.1021/acssensors.0c00694
ACS Sens. 2020, 5, 1822−1830

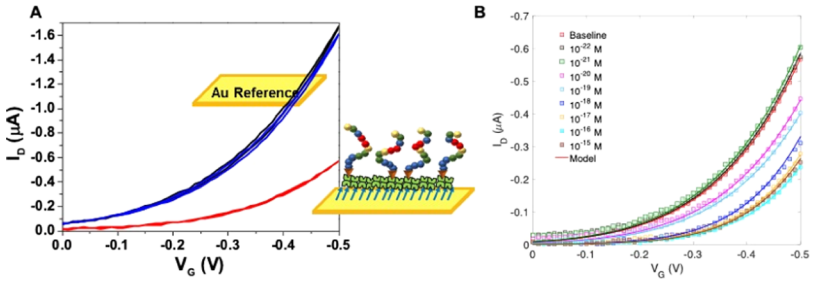

Figure 2. (A) Transfer $I-V$ characteristics (I_D as a function of V_G ranging from 0 to −0.5 V at V_D = −0.4 V) measured with a reference gold gate (black and blue curves) and the biofunctionalized one (red curve). The black and blue curves are registered on the same SiMoT device before and after recording the dose−response curve. The red curve corresponds to the single-strand oligonucleotide-functionalized gate incubated in the sole PBS solution. (B) SiMoT transfer $I-V$ curves measured upon exposure of the same gate to PBS standard solutions of target oligonucleotides at the following concentrations: 0.1 zM (black squares), 1 zM (green squares), 10 zM (magenta squares), 10^2 zM (dark cyan squares), 10^3 zM (blue squares), and 10^4 zM (dark yellow squares). The lines are relevant to the modeled transfer characteristics (I_D-V_G) as a function of the miR-182 nominal concentration (see the text for details).

TAACTCACACT), against the same biotinylated probe attached to the gate have been obtained by following the aforementioned protocol. All of the data points herein showed are averaged over three replicates and measured on three different resistors with three different gates. The resulting reproducibility error is computed as the standard deviation.

RESULTS AND DISCUSSION

A three-dimensional (3D) sketch of the SiMoT sensor is reported in Figure 1A. The EG-OTFT device comprises a channel (S and D contacts covered by a semiconductor) whose conductivity is controlled by the gate electrode (G) through HPLC-grade water, serving as the electrolyte medium. The gate surface has been biofunctionalized with a biotinylated single strand of oligonucleotides complementary to miR-s182, as depicted in Figure 1B.

This configuration, where the bioprobe has been attached on the gate surface instead of attaching it on the organic semiconductor (OSC) surface, has been selected to elude the generation of defects in the delocalized electronic system, impacting the charge carrier mobility. Moreover, the surface of the gold gate is morphologically and structurally more controlled and hence the biofunctionalization is more reproducible.[33] The application of the gate bias generates transient ionic currents, thus inducing the accumulation of electrolyte ions at the gate/electrolyte and electrolyte/semiconductor interfaces. The latter are addressed as charge double layers, possessing typical charge double layer capacitances. As these capacitances are on the order of tens of μF cm^{-2}, the SiMoT device can operate in the subvolt regime. The field-induced carriers result in an accumulated channel at the electrolyte/organic semiconductor interface, and the charge carriers injected at the source electrode into the OSC can eventually drift from S to D under the V_D bias. The core of the bioelectronic SiMoT sensor is the gate covered by the SAM of covalently attached biological recognition elements, depicted in Figure 1B. It is composed of mixed chem-SAM of carboxylic-terminated alkanethiols (chains) known to generate a dense coverage of proteins.[17] The carboxylic groups are then activated by means of EDC/sulfo-NHS chemistry before SAV is covalently attached. Chem-SAM is treated, afterward, with ethanolamine to block the activated and unreacted carboxylic groups, before the biotinylated single-strand oligonucleotides are segregated on the gate electrode, using the extraordinarily high binding affinity of SAV to the biotin molecule (dissociation constant in solution falling in the fM range). Upon ethanolamine blocking, amides groups can be eventually formed, which can originate hydrogen bonds connecting two neighboring chains. The blue arrows depicted in Figure 1B represent the dipole moments associated with each chem-SAM chain. The H-bond ensemble is supposed to form an electrostatic network that virtually connects all chains. The resultant dipole moment, holding its positive pole far from the gate surface, lowers its work function.[12] Indeed, the role of the H-bonding network has been already invoked to give a plausible explanation of single-molecule sensing;[13] however, no independent experimental evidence has yet been produced. Molecular dynamics simulations indicate that the introduction of a local defect, mimicking the binding event at the gate surface, generates a local disorder and the breakage of a few hydrogen bonds and that this occurrence triggers a cooperative domino effect that can, however, propagate only in the gating electric field.[26] Eventually, a switch of the 3-MPA layer into a new conformation state characterized by a lower work function is foreseen to occur. This assumption is experimentally substantiated by investigating the occurrence of an order−disorder phase transition in chem-SAM in the T = 20−80 °C range.[37,38] To this end, chem-SAM served as a working electrode in an electrochemical cell kept in a thermostatic bath. Different regimes, already identified in alkanethiols on gold in analogy to bilayer lipid vesicle phase transitions, have been observed on chem-SAM too. Indeed, below 30 °C, chem-SAM is very compact, as it greatly attenuates the rate of electron transfer between the water-soluble redox couple and the gold electrode. This is compatible with chem-SAM being very ordered, as resulted from the modeling reported elsewhere.[26] As the temperature increases above 30 °C, chem-SAM starts to progressively become more upstrained and elongated. The elongation of the chains is compatible with the occurrence of a gel/liquid crystal transition, involving the untilting of the chains probably due to H-bond loosening or even breaking. The propagation of the effect should be limited or inexistent in a SAM that is already untilted or completely disordered. The sensing measurements are performed by recording the SiMoT transfer curves, namely, I_D vs V_G at fixed V_D in the forward and reverse modes, after incubation of the biofunctionalized gate in the target oligonucleotide solution to be assayed. The device transfer characteristics are measured in water to maximize the Debye screening length and hence to minimize the screening of the electrostatic effects we are measuring with FET. The I_D-V_G transfer characteristics at V_D = − 0.4 V are reported in

https://dx.doi.org/10.1021/acssensors.0c00694
ACS Sens. 2020, 5, 1822−1830

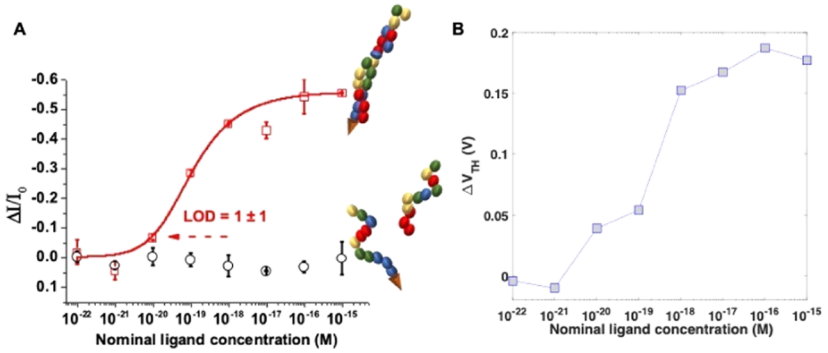

Figure 3. (A) Dose−response curve for the complementary single-strand oligonucleotides miR-182 (red squares) measured in PBS. The negative control dose−response curve involving the sensing of target oligonucleotides strand with one single mismatch is displayed as black circles. The data points are relevant to three replicates of the dose−response curves and the line to the modeling (see the text for details), while the error bars are calculated as the standard deviation. (B) Threshold voltage variation ΔV_{TH} as a function of the miR-182 nominal concentration. The concentration equal to 10^{-20} M corresponds to a single oligonucleotide into the solution used for gate incubation.

Figure 2A. The curves were measured in the forward and reverse modes to evaluate the hysteresis, minimized by selecting the inspected voltage window away from the potential where the electrochemical process occurred.[3]

Interestingly, the gate current I_G was monitored during the whole sensing measurement, ensuring that it remains at least 2 orders of magnitude lower than I_D. The black curve in Figure 2A is the I_D measured with the reference gold gate after the stabilization of the resistor, carried out by cycling the transistor in the gate voltage window ranging from 0 to −0.5 V, until at least three subsequent current traces perfectly overlap.[39] The current measured when the gold electrode was functionalized with the single-strand oligonucleotide probe serves as the gate and is reported in red. A change in the threshold voltage (V_T) or, equivalently, the gate work function of about 80 mV was observed. The blue curve is the I_D registered on the very same transistor channel comprising the reference gate used to measure the black curve, immediately after performing the measurement of the target oligonucleotide dose−response curve. It can be clearly observed the blue and black curves do not show any significant difference. This control experiment is important as the biofunctionalized gate undergoes an irreversible change of its electrostatic properties after the dose−response curve measurement, being the sensing process irreversible. Hence, the level of I_D flowing in the P3HT channel needs to be controlled by means of an independent reference gate before and after the sensing to validate the sensing response. The degree of change of the I_D current level, measured with the reference gate before and after the sensing, has been considered acceptable, as it has been found equal to 3%. In fact, it will be demonstrated that the limit of detection (LOD) of the sensing response is as high as 10%. The typical transfer curves measured after incubation of the same gate electrode biofunctionalized with the oligonucleotides probe into increasingly more concentrated target oligonucleotides samples are reported in Figure 2B. The red squares are relevant to the baseline (I_0), which has been measured upon incubation of the biofunctionalized gate in the PBS sample solution. Moreover, the black and green squares correspond to the incubation in the 0.1 zM and 1 zM target oligonucleotide solution, correspondingly. These latter nominal ligand concentrations correspond to 0 molecules in the sampled solutions. In fact, the black and green squares do not show any significant difference compared to the baseline. The magenta squares have been recorded upon incubation in a target oligonucleotide nominal concentration of 10 zM, corresponding to 1 ± 1 molecule in 100 μL of sampled solution. The error in the number of oligonucleotide probes sampled in 100 μL has been estimated considering both the Poisson and dilution errors. The total error for each assayed sample is calculated as the square root of the sum of the squares of the dilution and Poisson's uncertainties and has been extensively discussed elsewhere.[12] Remarkably, as it is apparent already from Figure 2B, a measurable relative change in the current of about 10% is clearly observed already at a concentration of 10 zM. In fact, the relative current change measured on the reference gate, before and after the sensing, is much lower, being 3%. This error level was used to validate each calibration curve, proving that the current variations measured at extremely low ligand concentrations are due to the selective hybridization biochemical interactions and not to spurious effects such as the organic semiconductor degradation. As clearly shown in Figure 2B, the current decrease is reproduced as the standard solutions at increased target oligonucleotide (miR-182) concentrations are subsequently analyzed. The saturation of the response has been achieved already at a nominal ligand concentration of 10^4 zM (10^{-18} M, 1 aM). The whole dose−response curve for oligonucleotide strands (miR-182) in PBS is shown in Figure 3A, as red squares, while the full line results from the SiMoT dose−response curve modeling are reported elsewhere.[26,27] This model for the dose−response curves has been conceived considering the Poisson distribution probability of single binding occurrences. The model foresees the SAM constituted by domains comprising a certain number of capturing oligonucleotides. If one target molecule binds to any of the biorecognition elements in one domain, this binding event is assumed to cause a shift in the work function of the whole domain, ϕ, induced by collaborative interactions propagating the variation. The process is assumed to be irreversible and stable as no other change in ϕ is possible, within that domain. The model further foresees that the more compact, or electrostatically connected, the SAM, the larger the domain generated upon interaction with the first single target molecule and the steeper the dose−response curve in the single-molecule range. To ensure that the SiMoT response is due only to the presence of the target oligonucleotide sequence in the investigated sample, the following negative control experiment has been performed. The biofunctionalized gate has been exposed to an oligonucleotide sequence with one single mismatch at position 14 compared to the miR-182 target

https://dx.doi.org/10.1021/acssensors.0c00694
ACS Sens. 2020, 5, 1822−1830

sequence. As can be seen from the data displayed in Figure 3A as black circles, the response is indeed zero and the negative control dose−response curve does not show an appreciable signal, clearly demonstrating the specificity of the single-strand oligonucleotide interaction with the complementary strand only. Each data point plotted in Figure 3A has been evaluated as the average of the dose−response curves evaluated on three resistors measured by three different biofunctionalized gates. Moreover, the relevant error bars have been calculated as the standard deviation, being at most 5%. This clearly reveals excellent interdevice reproducibility. The analysis of the dose curves of Figure 3A invariably shows also that a sizable change of I_D is registered already at 10 zM. According to the IUPAC definition of the limit of detection (LOD), considering the noise level and the standard deviation of the control experiment, a LOD level of 7% has been estimated. The LOD has been evaluated as the concentration that corresponds to a response of $(\Delta I/I_0)_{mean} \pm k\sigma$, where $(\Delta I/I_0)_{mean}$ is the average response of the blank sample, σ is the standard deviation, and k is a numerical factor selected according to the level of confidence required. IUPAC advises a value of $k = 3$ as the probability of the blank signal being threefold higher than the $(\Delta I/I_0)_{mean}$ (i.e., a false positive) is less than 1%.[40] In the model for the sensing curve in Figure 3A, the LOD level matches with the target DNA nominal concentration of 10 zM. This means that a measurable signal is produced when as low as 1 ± 1 target miR-182/complementary single-strand oligonucleotide complexes are formed. Hence, the hybridization of a single copy of miR-182 to one of the complementary probes attached to the gate surface is detected, with a time to result of about 4 h.

To further investigate the operation of the EG-OTFT biosensor, we developed a physically based model of the EG-OTFT biosensors to predict the measured transfer characteristics as a function of the miR-182 concentration. According to the state of the art, the charge transport into the P3HT OTFTs can be described by considering the energy disorder of the polymer chains.[41−44] In organic semiconductors, the localized density of states (DOS) is well described by an exponential function $g_L(E) = N_t/E_t \exp[(E - E_{HOMO})/E_t]$, where E is the energy, E_{HOMO} is the energy of the highest occupied molecular orbital (HOMO), N_t is the total density of localized states, and E_t is the energy disorder of the polymer. The current flowing from the source to the drain can be calculated as[45,46]

$$I_D = \frac{W}{L}\int_{V_S}^{V_D}\int_{V_{CH}}^{\varphi_S}\frac{q\mu_0 N_{HOMO}\exp\left\{\frac{q(\varphi - V_{CH}) - (E_{HOMO} - E_{Fi})}{K_B T}\right\}}{\sqrt{\frac{2q}{\varepsilon_S}\int_{V_{CH}}^{\varphi}\left[\int_{E_{HOMO}}^{E_{LUMO}} g_L(E) f_D(E, E_F)\mathrm{d}E\right]\mathrm{d}\varphi}}\mathrm{d}\varphi\,\mathrm{d}V_{CH} \quad (1)$$

where W and L are the channel width and length, respectively, V_S and V_D are the source and drain voltages, respectively (V_S = 0 V is the reference voltage), φ_S is the surface potential at the electrolyte−organic semiconductor interface, V_{CH} is the channel potential, q is the elementary charge, μ_0 is the hole mobility in the delocalized states, N_{HOMO} is the total density of HOMO states, φ is the electrostatic potential, E_{Fi} is the intrinsic Fermi energy level, K_B is the Boltzmann constant, T is the temperature, ε_S is the semiconductor permittivity, E_{LUMO} is the energy of the lowest unoccupied molecular orbital (LUMO), $g_L(E)$ is the localized DOS, $f_D(E,E_F)$ is the Fermi−Dirac occupation probability, and $E_F = q(\varphi - V_{CH}) - (E_{HOMO} - E_{Fi})$ is the quasi-Fermi energy. The organic semiconductor is coupled to the electrolyte to account for the electric field displacement. More in detail, the total surface density of ions accumulated in the electrolyte at the electrolyte/semiconductor interface has to be compensated by the surface density of holes accumulated in the transistor channel, and the continuity equation reads

$$C_{EL}\left[\frac{C_{BIO}}{C_{BIO} + C_{EL}}(V_G - V_{TH}) - \varphi_S\right] = \sqrt{\frac{2q}{\varepsilon_S}\int_{V_{CH}}^{\varphi_S}\left[\int_{E_{HOMO}}^{E_{LUMO}} g_L(E) f_D(E, E_F)\mathrm{d}E\right]\mathrm{d}\varphi} \quad (2)$$

where C_{EL} is the electrolyte/organic semiconductor capacitance per unit area, C_{BIO} is the biolayer/electrolyte capacitance per unit area, V_G is the gate voltage, and V_{TH} is the threshold voltage accounting for the functionalized gate work function and energy level of the materials used for the EG-OTFT fabrication. According to the design considerations and analyses developed in refs 3, 26, we designed the EG-OTFT biosensor with a gate area 20 times larger than the semiconductor area; hence, $C_{BIO} \gg C_{EL}$ with $C_{BIO}/(C_{BIO} + C_{EL}) = 1$. We note that this condition maximizes the biosensor sensitivity to the variations of the threshold voltage.[3] In other words, the device is by design extremely sensitive to electrostatic changes in the SAM and hence only V_T changes are measured. In fact, the V_T shifting toward more negative potentials is correlated to the decrease in the gate work function (ϕ) after the affinity binding. The decrease in ϕ is generated by the electrostatic effect of a dipole directed along the z-axis while segregated on the gate surface, pointing away from it with its positive pole.[26] By solving eqs 1 and eqs 1, we calculate the drain current as a function of the applied voltages V_G and V_D. The geometric and physical parameters of the model are listed in Table 1. More in detail, the geometric parameters are measured; the P3HT semiconductor parameter N_{HOMO} is provided by the first-principles pseudopotential density functional calculations[47] further validated with electrochemical measurements; and the physical parameters μ_0, N_t, E_t, and V_{TH} are obtained by reproducing the I_D-V_G characteristics measured before the biosensing experiments, viz., baseline, with the model (eqs 1 and eqs 1). We note that the extracted parameters are in full agreement with the state of the

Table 1. Geometric and Physical Parameters of the Drain Current Model

parameter	value	note
channel width	$W = 7650\ \mu m$	measured
channel length	$L = 5\ \mu m$	measured
temperature	$T = 294$ K	measured
HOMO energy level	$E_{HOMO} = 5.1$ eV	ref 36
LUMO energy level	$E_{LUMO} = 3.2$ eV	ref 36
total density of HOMO state	$N_{HOMO} = 1.4 \times 10^{18}$ cm^{-3}	ref 41
electrolyte/semiconductor capacitance	$C_{EL} = 6 \times 10^{-6}$ F cm^{-2}	fitted
hole mobility of delocalized states	$\mu_0 = 0.056$ cm^2 V^{-1} s^{-1}	fitted
total density of localized states	$N_t = 5.5 \times 10^{19}$ cm^{-3}	fitted
energy disorder	$E_t = 62.4 \times 10^{-3}$ eV	fitted
threshold voltage before sensing	$V_{TH} = 0.65$ V	fitted

https://dx.doi.org/10.1021/acssensors.0c00694
ACS Sens. 2020, 5, 1822−1830

art.[34,36,37,48] Figure 2B shows the comparison between the measurements and the proposed model. The model perfectly reproduces the transfer curves versus the miR-182 concentration with the very same set of geometric and physical parameters (Table 1) and by changing only the threshold voltage V_{TH}. More in detail, Figure 3B shows that V_{TH} is independent of the nominal ligand concentration up to 10^{-21} M, then it systematically increases by increasing the miR-182 concentration, and saturation is obtained at concentrations higher than 10^{-17} M. These results are in full agreement and further corroborate the model of the dose−response curves (Figure 3A). Indeed, at concentrations up to 10^{-21} M, there is no target oligonucleotide in the assay solution, while at higher concentrations, the biorecognition event(s) affects a large number of probes due to the collaborative interactions, which, in turn, result in a macroscopic variation of the biofunctionalized electrode work function, viz., EG-OTFT threshold voltage. The saturation of the biosensor response is achieved when all of the probes of the various domains have been affected by the biorecognition events as readily displayed by V_{TH} (Figure 3B, concentrations higher than 10^{-17} M).

A tentative sensing mechanism, proposed elsewhere,[26] triggered by the affinity binding event, involves a work function change that is assumed to propagate in the gating field through the electrostatic hydrogen-bonding network. Although this model still needs further investigation, it can be applied also to the single-molecule detection of oligonucleotide sequences. In fact, it is acknowledged that hybridization reactions of the two complementary RNA strands are exothermic,[49] with the energy involved being on the order of tens of kJ mol^{-1}. We therefore might assume that the binding energy, at least partially, can be transferred from bio-SAM to chem-SAM, causing the 3-MPA and 11-MUA chain desorption as disulfides. In fact, this process requires an estimated energy of 100 kJ mol^{-1} for a generic alkanethiol pair.[50] The subsequent exposure of chem-SAM to a reductive potential, occurring during the measurement of the EG-OTFT transfer characteristics, can achieve its full desorption, thus possibly generating an irreversible defective region. Thus, an extremely small defective region generated in chem-SAM can trigger a work function variation, impacting the gate area by orders of magnitude wider, once the SAM is exposed to an electric field, as detailed elsewhere[26] by means of molecular dynamics simulations. The SiMoT biosensor herein proposed is label-free, compatible with low-cost fabrication procedure, and also allows the reliable and ultrahighly sensitive detection of single-strand oligonucleotides down to the physical limit. This report, along with the papers previously published by our group, namely, single-molecule level of detection of protein markers,[3,4,26−32] demonstrates the selective assay at the physical limit of both genomic and protein markers. Furthermore, the SiMoT device is entirely compatible with low-cost printing techniques, largely used for electronic device fabrication. Last but not least, this opens new possibilities for a novel single-molecule, label-free platform capable of detecting biomarkers of completely different origins.

CONCLUSIONS

We have demonstrated highly selective, single-molecule, label-free sensing of genomic biomarkers using the SiMoT biosensing platform based on an electrolyte-gated thin-film transistor. Till now, the SiMoT platform has been employed to detect only protein biomarkers, such as human immunoglobulin G and immunoglobulin M, C-reactive protein, and HIV1 p24 antigen. In this work, the SiMoT approach has been successfully used for the detection of a single copy of a genomic biomarker. As a prototypical example, the miR-182 biomarker for multiple sclerosis was chosen. Given the generality of the functionalization process, the method can be easily extended also to other biotinylated probes or recognition elements. Moreover, the SiMoT device exploits solution-processable semiconducting materials and device fabrication procedures that are fully compatible with scalable large area and printing techniques. Given the general approach involved in the biofunctionalization protocol of the gate electrode, the aforementioned biosensing platform has been proposed to detect a variety of protein markers at the physical limit. This report shows that SiMoT can also detect genomic biomarkers. Hence, SiMoT is a label-free platform that can detect both genomic and protein markers at the physical limit. We are not aware of another label-free, single-molecule platform being able to perform at this level. The improvement of the technical capabilities of bioelectronic platforms, offering clinicians the possibility to rely on label-free biomarker detection down to the physical limit, is foreseen to dramatically revolutionize the way healthcare is provided. The proposed analytical tool will enable clinicians to associate the tiniest increase in the given number of selected biomarkers with the progression of a disease, particularly at its early stage. Eventually, physicians will be able to identify the very moment at which the illness state begins, representing an extraordinary breakthrough in early point-of-care clinical diagnostics.

AUTHOR INFORMATION

Corresponding Author

Luisa Torsi − *The Faculty of Science and Engineering, Åbo Akademi University, 20500 Turku, Finland; Dipartimento di Chimica, Università degli Studi di Bari "Aldo Moro", 70125 Bari, Italy; CSGI (Centre for Colloid and Surface Science), 70125 Bari, Italy*; Phone: +39-080-5442092; Email: luisa.torsi@uniba.it

Authors

Eleonora Macchia − *The Faculty of Science and Engineering, Åbo Akademi University, 20500 Turku, Finland;* orcid.org/0000-0002-1534-7336

Kyriaki Manoli − *Dipartimento di Chimica, Università degli Studi di Bari "Aldo Moro", 70125 Bari, Italy;* orcid.org/0000-0002-7600-0977

Cinzia Di Franco − *Dipartimento di Chimica, Università degli Studi di Bari "Aldo Moro", 70125 Bari, Italy; CNR, Istituto di Fotonica e Nanotecnologie, 70125 Bari, Italy*

Rosaria Anna Picca − *Dipartimento di Chimica, Università degli Studi di Bari "Aldo Moro", 70125 Bari, Italy;* orcid.org/0000-0001-8033-098X

Ronald Österbacka − *The Faculty of Science and Engineering, Åbo Akademi University, 20500 Turku, Finland*

Gerardo Palazzo − *Dipartimento di Chimica, Università degli Studi di Bari "Aldo Moro", 70125 Bari, Italy; CSGI (Centre for Colloid and Surface Science), 70125 Bari, Italy;* orcid.org/0000-0001-5504-2177

Fabrizio Torricelli − *Dipartimento Ingegneria dell'Informazione, Università degli Studi di Brescia, 25121 Brescia, Italy*

Gaetano Scamarcio − *Dipartimento Interateneo di Fisica "M. Merlin", Università degli Studi di Bari "Aldo Moro", 70125*

https://dx.doi.org/10.1021/acssensors.0c00694
ACS Sens. 2020, 5, 1822−1830

Bari, Italy; CNR, Istituto di Fotonica e Nanotecnologie, 70125 Bari, Italy

Complete contact information is available at: https://pubs.acs.org/10.1021/acssensors.0c00694

Funding

"OrgBIO" Organic Bioelectronics (PITN-GA-2013-607896), PON SISTEMA (MIUR), H2020—Electronic Smart Systems—SiMBiT: Single molecule bio-electronic smart system array for clinical testing (Grant agreement no. 824946), Future in Research APQ Ricerca Regione Puglia "Programma regionale a sostegno della specializzazione intelligente e della sostenibilità sociale ed ambientale—FutureInResearch"—"BEND" Biosensori elettronici intelligenti per la diagnosi precoce di malattie neurodegenerative (B164PG8), "PMGB-Sviluppo di piattaforme meccatroniche, genomiche e bioinformatiche per l'oncologia di precisione"—ARS01_01195—PON "RICERCA E INNOVAZIONE" 2014−2020 projects and CSGI are acknowledged for partial financial support.

Notes

The authors declare no competing financial interest.

■ ACKNOWLEDGMENTS

The authors thank Maria Liguori and Sabino Liuni for useful discussions.

■ REFERENCES

(1) Atkinson, A.; Colburn, W.; Degruttola, V.; Demets, D.; Downing, G.; Hoth, D.; Oates, J.; Peck, C.; Schooley, R.; Spilker, B.; Woodcock, J.; Zeger, S. Biomarkers Definitions Working Group. Biomarkers and surrogate endpoints: Preferred definitions and conceptual framework. *Clin. Pharmacol. Ther.* **2001**, *69*, 89.

(2) Gooding, J. J.; Gaus, K. Single-Molecule Sensors: Challenges and Opportunities for Quantitative Analysis. *Angew. Chem., Int. Ed.* **2016**, *55*, 11354−11366.

(3) Picca, R. A.; Manoli, K.; Macchia, E.; Sarcina, L.; Di Franco, C.; Cioffi, N.; Blasi, D.; Österbacka, R.; Torricelli, F.; Scamarcio, G.; Torsi, L. Ultimately Sensitive Organic Bioelectronic Transistor Sensors by Materials and Device Structures. *Adv. Funct. Mater.* **2019**, *4*, No. 1904513.

(4) Macchia, E.; Picca, R. A.; Manoli, K.; Di Franco, C.; Blasi, D.; Sarcina, L.; Ditaranto, N.; Cioffi, N.; Osterbacka, R.; Scamarcio, G.; Torricelli, F.; Torsi, L. Design About the amplification factors in organic bioelectronic sensors. *Mater. Horiz.* **2020**, *7*, 999−1013.

(5) Giljohann, D. A.; Mirkin, C. A. Drivers of biodiagnostic development. *Nature* **2009**, *46*, 461−464.

(6) Ginsburg, G. S.; Haga, S. B. Translating genomic biomarkers into clinically useful diagnostics. *Expert Rev. Mol. Diagn.* **2006**, *6*, 179−191.

(7) Golub, T. R.; Slonim, D. K.; Tomayo, P.; Huard, C.; Gaasenbeek, M.; Mesirov, J. P.; Coller, H.; Loh, M. L.; Downing, J. R.; Caligiuri, M. A.; et al. Molecular classification of cancer: class discovery and class prediction by gene expression monitoring. *Science* **1999**, *286*, 531−537.

(8) van de Vijver Marc, J.; He, Y. D.; van't Veer, L. J.; Dai, H.; Hart, A. A. M.; Voskuil, D. W.; Schreiber, G. J.; Peterse, J. L.; Roberts, C.; Marton, M. J.; et al. A gene-expression signature as a predictor of survival in breast cancer. *N. Engl. J. Med.* **2002**, *347*, 1999−2009.

(9) Hu, N.; Wang, C.; Hu, Y.; Yang, H. H.; Giffen, C.; Tang, Z. Z.; Han, X. Y.; Goldstein, A. M.; Emmert-Buck, M. R.; Buetow, K. H.; et al. Genome-Wide Association Study in Esophageal Cancer Using GeneChip Mapping 10K Array. *Cancer Res.* **2005**, *65*, 2542−2546.

(10) Esposito, I.; Segler, A.; Steiger, K.; Kloppel, G. Pathology, genetics and precursors of human and experimental pancreatic neoplasms: An update. *Pancreatology* **2015**, *15*, 598−610.

(11) Tufekci, K. U.; Oner, M. G.; Genc, S.; Genc, K. MicroRNAs and Multiple Sclerosis. *Autoimmune Dis.* **2011**, *807*, 1−27.

(12) Bartel, D. P. MicroRNAs: Target Recognition and Regulatory Functions. *Cell* **2009**, *136*, 281−297.

(13) Kanwar, J. R.; Mahidhara, G.; Kanwar, R. K. MicroRNA in human cancer and chronic inflammatory diseases. *Front. Biosci.* **2010**, *2*, 1113−1126.

(14) Sonntag, K. C. MicroRNAs and deregulated gene expression networks in neurodegeneration. *Brain Res.* **2010**, *1338*, 48−57.

(15) Otaegui, D.; Baranzini, S. E.; Armañanzas, R.; Calvo, B.; Muñoz-Culla, M.; Khankhanian, P.; Inza, I.; Lozano, J. A.; Castillo-Triviño, T.; Asensio, A.; et al. Differential micro RNA expression in PBMC from multiple sclerosis patients. *PLoS One* **2009**, *4*, No. e6309.

(16) Compston, A.; Coles, A. The window of therapeutic opportunity in multiple sclerosis. *Lancet* **2002**, *359*, 1221−1231.

(17) Freiesleben, S.; Hecker, M.; Zettl, U. K.; Fuellen, G.; Taher, L. Analysis of microRNA and Gene Expression Profiles in Multiple Sclerosis: Integrating Interaction Data to Uncover Regulatory Mechanisms. *Sci. Rep.* **2016**, *6*, No. 34512.

(18) Siegel, S. R.; Mackenzie, J.; Chaplin, G.; Jablonski, N. G.; Griffiths, L. Circulating microRNAs involved in multiple sclerosis. *Mol. Biol. Rep.* **2012**, *39*, 6219−6225.

(19) Keller, A.; Leidinger, P.; Steinmeyer, F.; Stähler, C.; Franke, A.; Hemmrich-Stanisak, G.; Kappel, A.; Wright, I.; Dörr, J.; Paul, F.; et al. Comprehensive analysis of microRNA profiles in multiple sclerosis including next-generation sequencing. *Mult. Scler.* **2014**, *20*, 295−303.

(20) Kawai, T.; Akira, S. The role of pattern-recognition receptors in innate immunity: update on Toll-like receptors. *Nat. Immunol.* **2010**, *11*, 1057−1063.

(21) Chen, C.; Zhou, Y.; Wang, J.; Yan, Y.; Peng, L.; Qiu, W. Dysregulated MicroRNA Involvement in Multiple Sclerosis by Induction of T Helper 17 Cell Differentiation. *Front. Immunol.* **2018**, *9*, 1256.

(22) Heid, C. A.; Stevens, J.; Livak, K. J.; Williams, P. M. Real time quantitative PCR. *Genome Res.* **1996**, *6*, 986−994.

(23) Raeymaekers, L. Basic principles of quantitative PCR. *Genome Res.* **1995**, *5*, 91−94.

(24) Schuster, S. C. Next-generation sequencing transforms today's biology. *Nat. Methods* **2008**, *5*, 16−18.

(25) Quail, M. A.; Smith, M.; Coupland, P.; Otto, T. D.; Harris, S. R.; Connor, T. R.; Bertoni, A.; Swerdlow, H. P.; Gu, Y. A tale of three next generation sequencing platforms: comparison of Ion Torrent, Pacific Biosciences and Illumina MiSeq sequencers. *BMC Genomics* **2012**, *13*, 341.

(26) Macchia, E.; Manoli, K.; Holzer, B.; Di Franco, C.; Ghittorelli, M.; Torricelli, F.; Alberga, D.; Mangiatordi, G. F.; Palazzo, G.; Scamarcio, G.; Torsi, L. Single-molecule detection with a millimetre-sized transistor. *Nat. Commun.* **2018**, *9*, No. 3223.

(27) Macchia, E.; Tiwari, A.; Manoli, K.; Holzer, B.; Ditaranto, N.; Picca, R. A.; Cioffi, N.; Di Franco, C.; Palazzo, G.; Scamarcio, G.; Torsi, L. Label-Free and Selective Single-Molecule Bioelectronic Sensing with a Millimeter-Wide Self-Assembled Monolayer of Anti-Immunoglobulins. *Chem. Mater.* **2019**, *31*, 6476−6483.

(28) Macchia, E.; Manoli, K.; Holzer, B.; Di Franco, C.; Picca, R.; Cioffi, N.; Scamarcio, G.; Palazzo, G.; Torsi, L. Selective single-molecule analytical detection of C-reactive protein in saliva with an organic transistor. *Anal. Bioanal. Chem.* **2019**, *411*, 4899−4908.

(29) Macchia, E.; Manoli, K.; Di Franco, C.; Scamarcio, G.; Torsi, L. New trends in single-molecule bioanalytical detection. *Anal. Bioanal. Chem.* **2020**, 1−10.

(30) Nature highlights- Selections from the scientific literature. *Nature*, 2018, *560*, 412.

(31) Sailapu, S. K.; Macchia, E.; Merino-Jimenez, I.; Esquivel, J. P.; Sarcina, L.; Scamarcio, G.; Minteer, S. D.; Torsi, L.; Sabaté, N. Standalone operation of an EGOFET for ultra-sensitive detection of HIV. *Biosens. Bioelectron.* **2020**, *156*, No. 112103.

(32) Macchia, E.; Sarcina, L.; Picca, R. A.; Manoli, K.; Di Franco, C.; Scamarcio, G.; Torsi, L. Ultra-low HIV-1 p24 detection limits with a bioelectronic sensor. *Anal. Bioanal. Chem.* **2020**, *412*, 811−818.

(33) Lin, Y.; Liu, C.-F.; Song, Y.-J.; Yang, L.; Zeng, W.-J.; Lai, W.-Y.; Huang, W. Improved performances of inkjet-printed poly(3-

hexylthiophene) organic thin-film transistors by inserting an ionic self-assembled monolayer. *RSC Adv.* **2016**, *6*, 40970−40974.
(34) Zare Bidoky, F.; Hyun, W. J.; Song, D.; Frisbie, C. D. Printed, 1 V electrolyte-gated transistors based on poly(3-hexylthiophene) operating at>10 kHz on plastic. *Appl. Phys. Lett.* **2018**, *113*, No. 053301.
(35) Jung, E. M.; Lee, S. W.; Kim, S. H. Printed ion-gel transistor using electrohydrodynamic (EHD) jet printing process. *Org. Electron.* **2018**, *52*, 123−129.
(36) Holzer, B.; Manoli, K.; Ditaranto, D.; Macchia, E.; Tiwari, A.; Di Franco, C.; Scamarcio, G.; Torsi, L. Characterization of Covalently Bound Anti-Human Immunoglobulins on Self-Assembled Monolayer Modified Gold Electrodes. *Adv. Biosyst.* **2017**, No. 1700055.
(37) Badia, A.; Back, R.; Lennox, R. B. Phase Transitions in Self-Assembled Monolayers Detected by Electrochemistry. *Angew. Chem., Int. Ed* **1994**, *22*, 2332−2334.
(38) Badia, A.; Lennox, R. B.; Reven, L. A. Dynamic View of Self-. Assembled Monolayers. *Acc. Chem. Res.* **2000**, *33*, 475.
(39) Manoli, K.; Patrikoussakis, M. M.; Magliulo, M.; Dumitru, L. M.; Mulla, M. Y.; Sabbatini, L.; Torsi, L. Pulsed voltage driven organic field-effect transistors for high stability transient current measurements. *Org. Electron.* **2014**, *15*, 2372−2380.
(40) Torsi, L.; Magliulo, M.; Manoli, K.; Palazzo, G. Organic Field-Effect Transistors: a Tutorial Review. *Chem. Soc. Rev.* **2013**, *42*, 8612−8628.
(41) Rivnay, J.; Noriega, R.; Northrup, J. E.; Kline, R. J.; Toney, M. F.; Salleo, A. Structural origin of gap states in semicrystalline polymers and the implications for charge transport. *Phys. Rev. B* **2011**, *83*, No. 121306(R).
(42) Hong, K.; Kim, S. H.; Mahajan, A.; Frisbie, C. D. Performance and Stability of Aerosol-Jet-Printed Electrolyte-Gated Transistors Based on Poly(3-hexylthiophene). *ACS Appl. Mater. Interfaces* **2014**, *6*, 18704−18711.
(43) Wang, C.; Jimison, L. H.; Goris, L.; McCulloch, I.; Heeney, M.; Ziegler, A.; Salleo, A. Microstructural Origin of High Mobility in High-Performance Poly(thieno-thiophene) Thin-Film Transistors. *Adv. Mater.* **2010**, *22*, 697−701.
(44) Servati, P.; Nathan, A.; Amaratunga, G. A. J. Generalized transport-band field-effect mobility in disordered organic and inorganic semiconductors. *Phys. Rev. B* **2006**, *74*, No. 245210.
(45) Torricelli, F. Charge transport in organic transistors accounting for a wide distribution of carrier energies—Part I: theory. *IEEE Trans. Electron Devices* **2012**, *59*, 1514−1519.
(46) Torricelli, F.; Colalongo, L.; Raiteri, D.; Kova′cs-Vajna, Z. M.; Cantatore, E. Ultra-high gain diffusion-driven organic transistor. *Nat. Commun.* **2016**, *7*, No. 10550.
(47) Northrup, J. E. Atomic and electronicstructure of polymer organic semiconductors: P3HT, PQT, and PBTTT. *Phys. Rev. B* **2007**, *76*, No. 245202.
(48) Kergoat, L.; Herlogsson, L.; Braga, D.; Piro, B.; Pham, M. C.; Crispin, X.; Berggren, M.; Horowitz, G. A water-gate organicfield-effect transistor. *Adv. Mater.* **2010**, *22*, 2565−2569.
(49) Harrison, J. G.; Balasubramanian, S. Synthesis and hybridization analysis of a small library of peptide−oligonucleotide conjugates. *Nucleic Acids Res.* **1998**, *26*, 3136−3145.
(50) Wano, H.; Uosaki, K. In situ, real-time monitoring of the reductive desorption process of self-assembled monolayers of hexanethiol on Au(111) surfaces in acidic and alkaline aqueous solutions by scanning tunneling microscopy. *Langmuir* **2001**, *17*, 8224−8228.

https://dx.doi.org/10.1021/acssensors.0c00694
ACS Sens. 2020, 5, 1822−1830